Graphene-Reinforced MOFs

Deutsche Ausgabe: DOI: 10.1002/ange.201603320
Internationale Ausgabe: DOI: 10.1002/anie.201603320

Remarkable Improvement in the Mechanical Properties and CO_2 Uptake of MOFs Brought About by Covalent Linking to Graphene

*Ram Kumar, Devaraj Raut, Upadrasta Ramamurty, and C. N. R. Rao**

Abstract: *Metal–organic frameworks (MOFs) are exceptional as gas adsorbents but their mechanical properties are poor. We present a successful strategy to improve the mechanical properties along with gas adsorption characteristics, wherein graphene (Gr) is covalently bonded with M/DOBDC (M = Mg^{2+}, Ni^{2+}, or Co^{2+}, DOBDC = 2,5-dioxido-1,4-benzene dicarboxylate) MOFs. The surface area of the graphene–MOF composites increases up to 200–300 $m^2 g^{-1}$ whereas the CO_2 uptake increases by ca. 3–5 wt% at 0.15 atm and by 6–10 wt% at 1 atm. What is significant is that the composites exhibit improved mechanical properties. In the case of Mg/DOBDC, a three-fold increase in both the elastic modulus and hardness with 5 wt% graphene reinforcement is observed. Improvement in both the mechanical properties and gas adsorption characteristics of porous MOFs on linking them to graphene is a novel observation and suggests a new avenue for the design and synthesis of porous materials.*

Metal–organic frameworks (MOFs) are important materials with potential application in gas storage, separation, and catalysis.[1] MOFs are expected to decrease the energy penalty of CO_2 capture from flue gas in coal-fired power plants.[2] For CO_2 capture and long-term performance in these applications, the material should be chemically and mechanically stable to allow dense packing of the adsorbent bed without loss of the porous network.[2b] For CO_2 separation from post-combustion flue gas, hydrothermal stability of the MOFs is an important factor.[2b,3] Most of the low-density (density $< 1\ g\,cm^{-3}$) porous open frameworks are not mechanically robust with an elastic modulus of 3–4 GPa and hardness of 200–500 MPa.[3,4] Inorganic zeolites have a low surface area in comparison to MOFs but have an elastic modulus of 40–100 GPa and a hardness of 2.5–10 GPa.[5] It is, therefore, highly desirable to adopt a strategy that would enhance the mechanical properties of MOFs without imposing a penalty on their intrinsic surface area and gas adsorption properties. In view of the excellent mechanical properties of graphene,[6] we have investigated selected MOFs covalently linked with graphene for mechanical properties and CO_2 uptake. It should be noted that there is some evidence for increased hydrothermal stability, enhanced gas adsorption and selectivity for gas separation in MOF-graphene composites.[7] We have synthesized composites of M/DOBDC or CPO-27-M, (M = Mg^{2+}, Ni^{2+} and Co^{2+} and DOBDC = 2,5-dioxido-1,4-benzene dicarboxylate) which have been reported to exhibit highest uptake of CO_2 at low pressure,[2c,8] covalently linked to graphene, and studied their surface area, gas storage (for both CO_2 and H_2), and mechanical properties.

The strategy employed by us involves benzoic acid functionalization of the graphene basal plane. The carboxylate groups of the benzoic acid functionalized graphene (BFG) bond with metal ions just as the carboxylate groups in DOBDC linker. Although Mg/DOBDC has the highest low-pressure CO_2 uptake reported to date in the literature, the performance deteriorates significantly in the presence of moisture with the recovery of only 16% of its initial capacity after regeneration. Although Ni/DOBDC and Co/DOBDCs exhibit a smaller CO_2 uptake than Mg/DOBDC but show significant retention (61–85%) of uptake capacity after exposure and regeneration.[9] The results of present study of the different MOF-graphene composites demonstrate that it is possible to design composites that are highly functional and mechanically robust simultaneously.

Scheme 1 shows the steps involved in the synthesis of graphene reinforced-M/DOBDC composites (see Experimental Section in the Supporting Information for details). The composites (C) are denoted as MCGr-X where M = Mg^{2+}, Ni^{2+}, and Co^{2+} and X corresponds to the weight % of graphene incorporated (X = 2, 5, and 10 wt%). Figures S1 to S3 (Supporting Information) show powder X-ray diffraction (PXRD) patterns of the as-synthesized M/DOBDC and the MCGr-X composites. The PXRD patterns of MCGr-X are consistent with the reported pattern of isostructural M/DOBDC indexed on a trigonal cell.[8a,10] The M^{2+} ions are bridged by the carboxylate and oxy groups of the fully deprotonated 2,5-dihydroxybenzene-1,4-dicarboxylic acid, resulting in cross-linking chains arranged in a hexagonal manner. All the oxygen of the ligand are involved in coordination to the metal ions resulting in hexagonal 1D pore with an average cross-sectional channel dimension of approximately $1.1 \times 1.1\ nm^2$.[8a,10,11] The MOF matrix is uniformly reinforced by the large area 2D graphene sheets in all random directions. Parent MOF determines the structure, with graphene reinforcing the MOF matrix and we observe the same PXRD pattern for MCGr-X as pristine MOF.

Infrared spectra (IR) of methanol-exchanged MgCGr-X are shown in Figures S4 to S6. The spectra of all the MCGr-X show bands at 818, 1122, 1570, and 1637 cm^{-1} corresponding

[*] R. Kumar, Prof. C. N. R. Rao
Chemistry and Physics of Materials Unit, New Chemistry Unit, Sheikh Saqr Laboratory, International Centre for Materials Science (ICMS), and CSIR Centre of Excellence in Chemistry, Jawaharlal Nehru Centre for Advanced Scientific Research
Jakkur P.O. Bangalore-560064 (India)
E-mail: cnrrao@jncasr.ac.in
D. Raut, Prof. U. Ramamurty
Department of Materials Engineering, Indian Institute of Science
Bangalore-560012 (India)

Supporting information for this article can be found under: http://dx.doi.org/10.1002/anie.201603320.

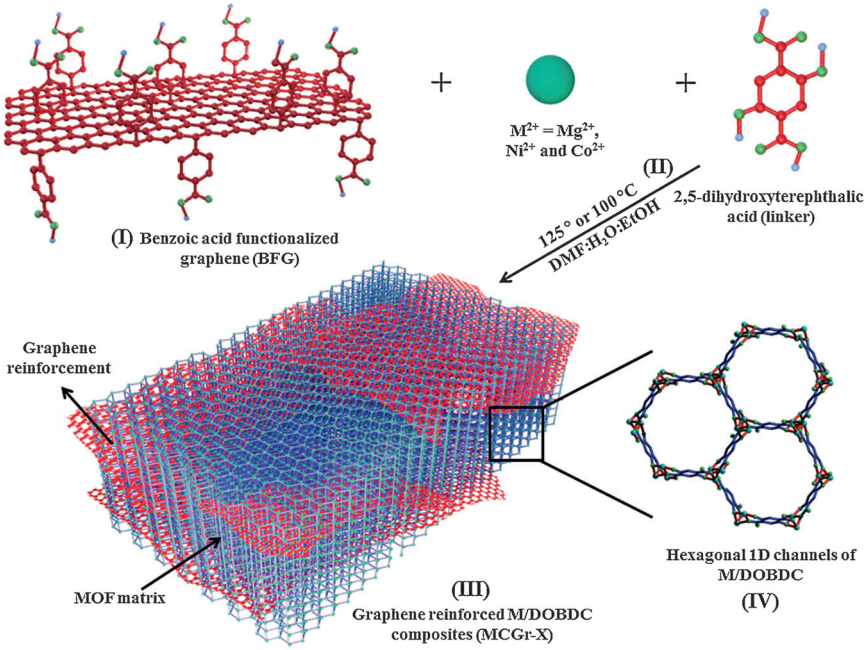

Scheme 1. Schematic representation of the synthesis of covalently linked MCGr-X composites. (I) Benzoic acid functionalized graphene (BFG). (II) In situ growth of M/DOBDC crystals on the graphene basal plane. (III) Graphene reinforced MCGr-X composites (M = Mg^{2+}, Ni^{2+}, and Co^{2+}; X = 0, 2, 5, and 10 wt%), where M is the metal ion and Gr-X different weight % of graphene reinforced in the M/DOBDC matrix. (IV) Hexagonal (ca. 1.1 × 1.1 nm^2) 1D channels of M/DOBDC.

to C–H out of plane bending, C–O stretch, C=C ring stretch and carboxylates attached to the metal center (Figure S4). The sharp band at 1415 cm^{-1} and the broad band around 3330 cm^{-1} are assigned to the C-O-H in-plane bend and hydrogen bonded O–H stretch of methanol trapped inside the 1D channel after solvent exchange.[12] Raman spectra of the MCGr-X composites show bands of the ligand and M–O stretching band (Figure 1, Figures S7 and S8).[12] The broad bands at 1343 and 1585 cm^{-1} merging with the MOF bands in the 1150–1670 cm^{-1} range arise from the D and G bands of graphene.[13] The intensities of these bands increase on increasing the graphene content. Thermogravimetric analysis of the MCGr-X composites in nitrogen shows the same thermal stability as the pristine MOFs (Figures S9–S11).

Figure 2 shows scanning and transmission electron microscope (SEM and TEM respectively) images of MgCGr-X samples. Pristine Mg/DOBDC comprises irregular shaped 10–20 μm crystals (Figure 2a). With the addition of 2 and 5 wt% graphene, rectangular crystals less than 10 μm are observed (Figures 2b and 2c). Although a smooth rectangular surface is observed in the case of MgCGr-2 and MgCGr-5, observation of the edges shows sandwiched graphene sheets between the MOF layers (Figure 2). Addition of 10 wt% graphene significantly alters the crystal morphology and we find 100–200 nm diameter MOF nanowires wrapped in a graphene matrix. Figure 3 shows SEM and TEM images of NiCGr-X samples. Pristine Ni/DOBDC has 5 to 10 μm flower shaped agglomerated morphology (Figure 3a). Addition of 2 wt% graphene gives rise to morphology similar to that of pristine Ni/DOBDC with the graphene sheets sandwiched in the MOF matrix (Figure 3b). Addition of 5 and 10 wt% graphene affects the nucleation and growth of Ni/DOBDC crystals significantly and we observe bean shaped 500 nm to 1 μm crystals sandwiched by graphene sheets (Figures 3c and 3d). A time-dependent study of crystal growth process shows the evolution of Ni/DOBDC crystals on graphene surface and its effect on the morphology (Figure S12).

Co/DOBDC has a mixture of rectangular and irregular 5–10 μm crystals (Figure S13) and addition of graphene leads to rectangular shaped crystals with graphene sandwiched between the layers for CoCGr-X crystals (Figure S13 and S14). Microscopic investigations clearly show uniform reinforcement of MOF matrix by large micron sized graphene sheets. The change in morphology and crystal size with the addition of graphene to the MOFs arises from coordination modulation[14]

Surface areas and porosities of MCGr-X (M = Mg^{2+}, Ni^{2+}, and Co^{2+}; X = 2, 5, and 10 wt% graphene) were

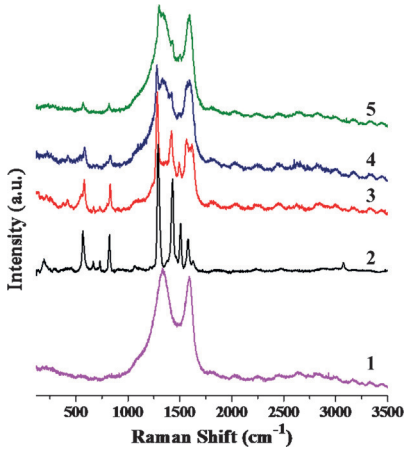

Figure 1. Raman spectra of 1) benzoic acid functionalized graphene, 2) Mg/DOBDC, 3) MgCGr-2, 4) MgCGr-5, and (5) MgCGr-10. Where, Gr-X (X = 2, 5, and 10 wt%) corresponds to different weight % of graphene reinforced in the Mg/DOBDC matrix.

determined by nitrogen adsorption at 77 K. Figure 4a shows the nitrogen adsorption–desorption and pore size distribution profiles of MgCGr-X and NiCGr-X. The results are summarized in Table 1 (see Table S1 for CoCGr-X data). The Brunauer–Emmet–Teller (BET) surface area of Mg/DOBDC is 1161 $m^2 g^{-1}$ whereas the surface areas of MgCGr-X samples are in the range of 1282–1474 $m^2 g^{-1}$ (Table 1), the surface area of the sample with 2 wt% graphene being highest. The pore volume increases from 0.54 $cm^3 g^{-1}$ for Mg/DOBDC to about 0.7 $cm^3 g^{-1}$ in the MgCGr-X composites (Table 1). A similar increase in surface

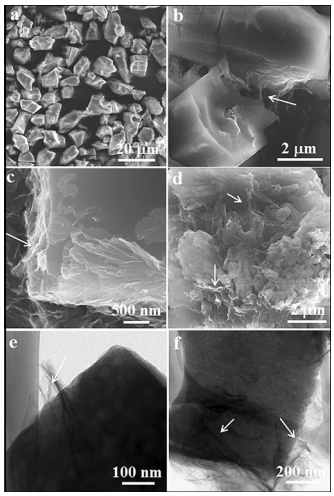

Figure 2. Scanning electron microscopy (SEM) images of a) Mg/DOBDC, b) MgCGr-2, c) MgCGr-5, and d) MgCGr-10. Transmission electron microscopy (TEM) images of e) MgCGr-2 and f) MgCGr-5. Arrows show graphene reinforced in the Mg/DOBDC MOF matrix.

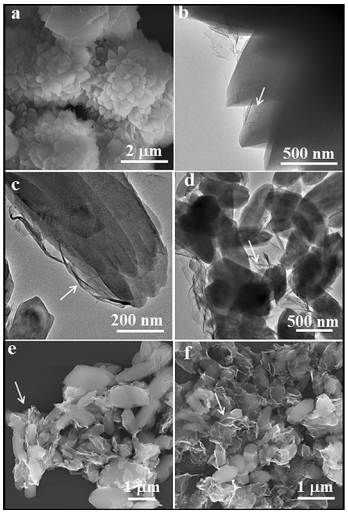

Figure 3. a) SEM image of Ni/DOBDC; TEM images of b) NiCGr-2, c) NiCGr-5, and d) NiCGr-10. SEM images of e) NiCGr-5 and f) NiCGr-10. Arrows show graphene reinforced in the Ni/DOBDC MOF matrix.

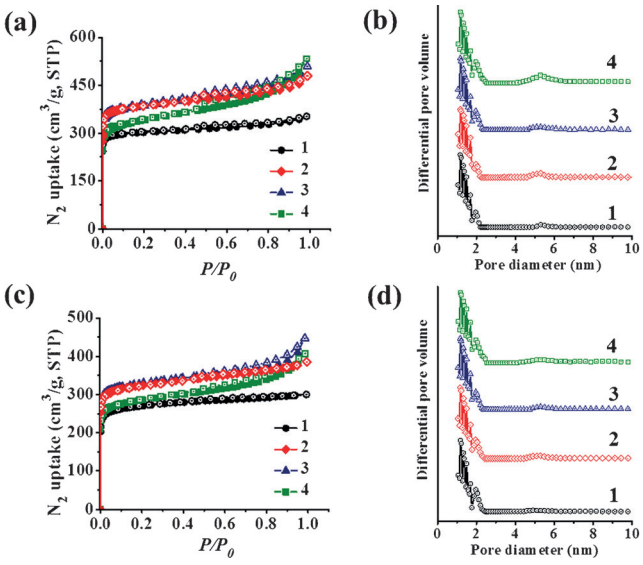

Figure 4. a),b) Nitrogen adsorption–desorption isotherms at 77 K and corresponding pore size distribution calculated using non-local density functional theory (NLDFT) of 1) Mg/DOBDC, 2) MgCGr-2, 3) MgCGr-5, and 4) MgCGr-10. c),d) Nitrogen adsorption–desorption isotherms at 77 K and corresponding pore size distribution calculated using (NLDFT) of 1) Ni/DOBDC, 2) NiCGr-2, 3) NiCGr-5, and 4) NiCGr-10.

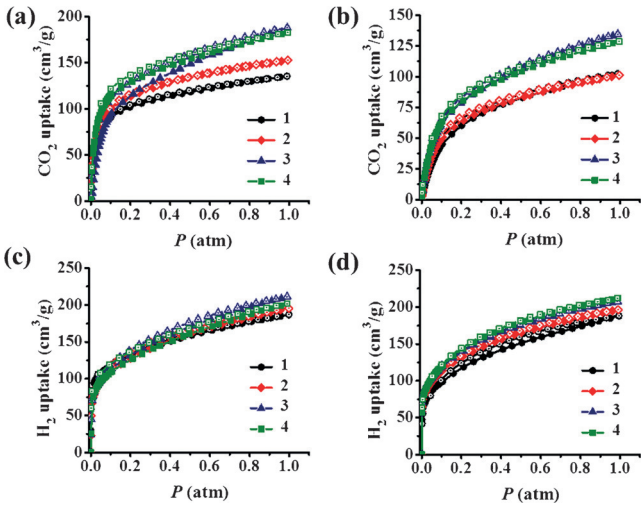

Figure 5. a) Carbon dioxide adsorption–desorption isotherms of 1) Mg/DOBDC, 2) MgCGr-2, 3) MgCGr-5, and 4) MgCGr-10 at 298 K. b) Carbon dioxide adsorption–desorption isotherms of 1) Ni/DOBDC, 2) NiCGr-2, 3) NiCGr-5, and 4) NiCGr-10 at 298 K. c) Hydrogen adsorption–desorption isotherms of 1) Mg/DOBDC, 2) MgCGr-2, 3) MgCGr-5, and 4) MgCGr-10 at 77 K. d) Hydrogen adsorption–desorption isotherms of 1) Ni/DOBDC, 2) NiCGr-2, 3) NiCGr-5, and 4) NiCGr-10 at 77 K.

area and pore volume are observed in NiCGr-X and CoCGr-X as well (Table 1 and Table S1). The lighter metal Mg in comparison to heavier transition-metal counterparts Ni and Co causes a higher surface area in a series of isostructural materials. Enhancement in the porous properties occurs up to a certain weight % of graphene, subsequent addition of graphene not leading to further enhancement. Pore size distribution of MCGr-X composites were calculated using non-local density functional theory (NLDFT) (Figure 4 and Figure S15).The pore sizes of MCGr-X are in 1–2 nm microporous range just as in pristine M/DOBDC. Thus, we see that the microporous feature and architectures of the frameworks are retained in the composites on addition of up to 10 wt % graphene.

Figures 5 and S16 show the CO_2 uptake profiles of MCGr-X ($M = Mg^{2+}$, Ni^{2+}, and Co^{2+}; $X = 2$, 5, and 10 wt % of graphene) at 298 K. Tables 1 and S1 summarize the CO_2 uptake data of the composites. Due to the relatively low concentration of CO_2 (15–16 %) in flue gas, the low pressure CO_2 uptake at pressure, $P \approx 0.15$ atm is of relevance for post-combustion CO_2 capture.[2b] MCGr-X composites exhibit an enhancement in CO_2 uptake at both $P \approx 0.15$ and 1 atm. Amongst the materials examined, MgCGr-X samples show the best low-pressure CO_2 uptake performance with pristine

Table 1: Summary of the Brunauer–Emmet–Teller (BET) surface areas, pore volume, CO_2 and H_2 uptake, CO_2/N_2 selectivity, and mechanical properties of the M/DOBDC and graphene reinforced MCGr-X composites.

Sample name	BET surface area [$m^2 g^{-1}$]; (Pore volume, $cm^3 g^{-1}$)	CO_2 uptake at 298 K $P = 0.15$ atm [wt%] and (wt% at $P = 1$ atm)	H_2 uptake at 77 K and 1 atm [wt%]	Initial slope CO_2/ Initial slope N_2 selectivity at 298 K	Elastic Modulus [GPa]; (Standard deviation, GPa)	Hardness [MPa]; (Standard deviation, MPa)
Mg/DOBDC	1161 (0.54)	19 (26.6)	1.6	123	11 (0.5)	569 (85)
MgCGr-2	1474 (0.72)	21.4 (30)	1.7	144	20.5 (0.78)	1167 (174)
MgCGr-5	1465 (0.72)	21 (37)	1.9	233	29.6 (0.98)	1730 (162)
MgCGr-10	1282 (0.7)	24 (35.7)	1.8	335	13.3 (1)	754 (225)
Ni/DOBDC	1022 (0.46)	10.4 (20)	1.7	86	7.7 (0.6)	345 (115)
NiCGr-2	1235 (0.57)	11.6 (19.8)	1.7	112	9.1 (0.57)	513 (145)
NiCGr-5	1257 (0.6)	14 (26)	1.8	154	12.1 (0.85)	696 (159)
NiCGr-10	1075 (0.56)	14.3 (25)	1.9	160	14.3 (0.9)	872 (213)

Mg/DOBDC showing an uptake of 19 wt%. The MgCGr-X samples exhibit a CO_2 uptake of 21–24 wt% at 0.15 atm (Table 1). At $P \approx 1$ atm, Mg/DOBDC shows an uptake of around 27 wt% whereas the MgCGr-X composites have an uptake of 30–37 wt%. The Co and Ni/DOBDC have an initial CO_2 uptake of about 10 wt%, whereas the CoCGr-X and NiCGr-X samples show an uptake in the range of around 11–14 wt% at $P \approx 0.15$ atm (Tables 1 and S1). At $P \approx 1$ atm, Ni/DOBDC has CO_2 uptake of 20 wt% whereas NiCGr-X samples have CO_2 uptake in the range of 20–25 wt% (Table 1). The Co/DOBDC has an uptake of 22 wt% whereas CoCGr-X samples have an uptake of 24–29 wt% at $P \approx 1$ atm (Table S1). Thus, the CO_2 uptake data of MCGr-X samples reveal an enhancement of approximately 3–5 wt% at $P \approx 0.15$ atm and an enhancement of around 6–10 wt% at $P \approx 1$ atm (Table 1 and S1). The significantly higher CO_2 uptake in Mg/DOBDC and composites in comparison to the Ni and Co counterparts is attributed to the increased ionic character of Mg–O bond which provides strong affinity and additional uptake of CO_2 beyond simple weight effects of the lighter metal.

We have examined the CO_2/N_2 adsorption selectivity by using the initial slope ratios (Henry's law constant) for single-component adsorption isotherms at 298 K (Table 1).[2a,15] This method is useful and convenient to compare the performances of different porous materials under similar conditions. The adsorption selectivity of Mg/DOBDC and corresponding different weight ratio composites are calculated by taking the ratio of low pressure region slopes of CO_2 and N_2 adsorption isotherms. CO_2/N_2 selectivity increases markedly on the addition of graphene (Table 1). The selectivity of Mg/DOBDC and MgCGr-2, 5, and 10 wt% composites are 123, 144, 233, and 335 respectively (Table 1 and Figure S17). The CO_2/N_2 selectivity values for Ni/DOBDC and NiCGr-2, 5, and 10 wt% composites are 86, 112, 154, and 160 respectively (Table 1 and Figure S18). The enhancement of CO_2 uptake and selectivity with the addition of graphene in the MOF matrix suggests a significant role of graphene.

Figure 5c,d shows the hydrogen uptake profiles of MgCGr-X and NiCGr-X samples (X = 2, 5, and 10 wt% of graphene) at 77 K. Mg/DOBDC has a H_2 uptake of 1.6 wt% at 1 atm whereas the composites show a marginal increase in the H_2 uptake, in the range of 1.7–1.9 wt% (see Table 1). A similar trend in hydrogen uptake is found for NiCGr-X and CoCGr-X samples, with the uptake in the range of 1.6–1.9 wt% (Tables 1 and S1). The marginal increase in the hydrogen uptake of composites is attributed to the enhanced surface area of the composites in comparison with the pristine MOF. From the CO_2 and H_2 uptake measurements, we conclude that dispersive forces provided by the π electron cloud of graphene may have an influence on quadrupolar CO_2 with a higher polarizability than H_2.

We have carried out mechanical property measurements on pellets of MCGr-X composites using the nanoindentation technique, and the results are summarized in Figure 6 and Table 1. The elastic modulus, E, and hardness, H, were extracted from the load-depth of penetration (P–h) curves (see Figures S22 and S23 for representative ones) using the standard Oliver-Pharr method. The E and H data are plotted as a function of the wt% graphene in the composite. In the case of NiCGr-X samples (Figure 6b), a linear increase in both E and H are noted, and the enhancements in both the

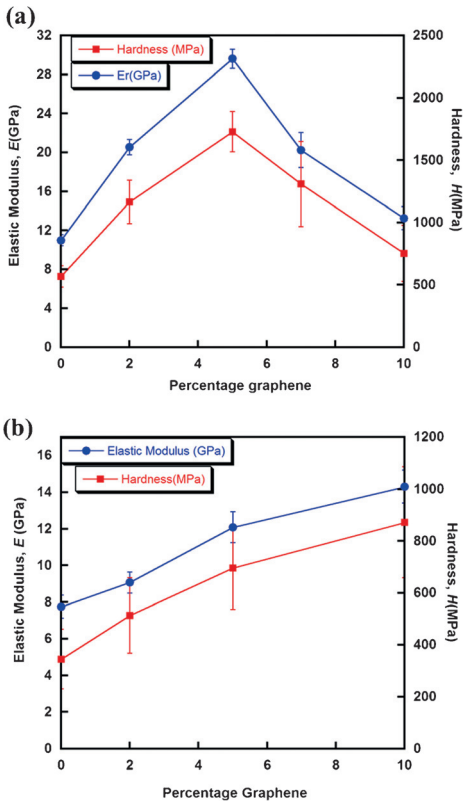

Figure 6. a) Elastic modulus and hardness of Mg/DOBDC and MgCGr-X, and b) Ni/DOBDC and NiCGr-X (X = different wt% of graphene reinforced in the M/DOBDC matrix).

properties are significant. For example, a 5 wt% addition of graphene to Ni/DOBDC enhances its *E* and *H* by 56% and 102% respectively. The observed enhancements are even more significant (at 170 and 204%) in the case of MgCGr-5. While continued increase of the graphene content to 10 wt% further enhances the Ni/DOBDC mechanical properties, the mechanical performance of Mg/DOBDC with 10 wt% is markedly inferior to those with 2 and 5 wt% graphene. Interestingly, some of the gas absorption characteristics of Mg/DOBDC-graphene composites also exhibit such a reversal when the graphene content is increased to 10 wt% (see for example, Figures 4a and 4b). A possible reason for this marked drop in both mechanical and functional properties in MgCGr-10 graphene composites could be the significant change in the crystal morphology and agglomeration of graphene in the MOF matrix at this reinforcement level, as already noted (Figure 2 and S21). The 7 wt% contrast sample confirms the effect of agglomeration in decreasing the mechanical properties. It should be noted that higher concentrations of graphene in polymer, metal and ceramic composites are known to degrade mechanical properties due to agglomeration.[16] Higher mechanical properties of Mg/DOBDC system in comparison to the Ni counterpart is attributed to increased ionic character of the Mg–O bond resulting in more robust framework. Nevertheless, the substantial enhancements in the mechanical properties that accrue due to 5 wt% graphene reinforcement demonstrate the utility of such a composite route for imparting mechanical robustness to the MOFs that are otherwise fragile in nature.

In summary, we have synthesized composites of M/DOBDC ($M = Mg^{2+}$, Ni^{2+}, and Co^{2+}; DOBDC = 2,5-dioxido-1,4-benzene dicarboxylate) covalently linked with different proportions of graphene, to examine if such composites exhibits enhancement in mechanical as well as functional properties. Our experimental results show that these composites possess significantly higher surface area, enhanced gas (both CO_2 and H_2) adsorption capability, and substantially improved elastic modulus and hardness. It appears that 5 wt% graphene reinforcement is optimal for the improvement of gas adsorption as well as mechanical properties. We feel that these results indicate a means to enhance the mechanical strength of MOFs without affecting their gas adsorption characteristics.

Keywords: CO_2 uptake · composite material · graphene · mechanical properties · metal–organic frameworks

How to cite: *Angew. Chem. Int. Ed.* **2016**, *55*, 7857–7861
Angew. Chem. **2016**, *128*, 7988–7992

[1] a) A. K. Cheetham, C. N. R. Rao, R. K. Feller, *Chem. Commun.* **2006**, 4780; b) J.-R. Li, R. J. Kuppler, H.-C. Zhou, *Chem. Soc. Rev.* **2009**, *38*, 1477; c) J. Lee, O. K. Farha, J. Roberts, K. A. Scheidt, S. T. Nguyen, J. T. Hupp, *Chem. Soc. Rev.* **2009**, *38*, 1450; d) H. Furukawa, K. E. Cordova, M. O'Keeffe, O. M. Yaghi, *Science* **2013**, *341*, 974.

[2] a) S. Keskin, T. M. van Heest, D. S. Sholl, *ChemSusChem* **2010**, *3*, 879; b) K. Sumida, D. L. Rogow, J. A. Mason, T. M. McDonald, E. D. Bloch, Z. R. Herm, T.-H. Bae, J. R. Long, *Chem. Rev.* **2012**, *112*, 724; c) A. Ö. Yazaydın, R. Q. Snurr, T.-H. Park, K. Koh, J. Liu, M. D. LeVan, A. I. Benin, P. Jakubczak, M. Lanuza, D. B. Galloway, J. J. Low, R. R. Willis, *J. Am. Chem. Soc.* **2009**, *131*, 18198.

[3] J. C. Tan, A. K. Cheetham, *Chem. Soc. Rev.* **2011**, *40*, 1059.

[4] a) J. C. Tan, T. D. Bennett, A. K. Cheetham, *Proc. Natl. Acad. Sci. USA* **2010**, *107*, 9938; b) D. F. Bahr, J. A. Reid, W. M. Mook, C. A. Bauer, R. Stumpf, A. J. Skulan, N. R. Moody, B. A. Simmons, M. M. Shindel, M. D. Allendorf, *Phys. Rev. B* **2007**, *76*, 184106; c) T. D. Bennett, J.-C. Tan, S. A. Moggach, R. Galvelis, C. Mellot-Draznieks, B. A. Reisner, A. Thirumurugan, D. R. Allan, A. K. Cheetham, *Chem. Eur. J.* **2010**, *16*, 10684; d) Y. H. Hu, L. Zhang, *Phys. Rev. B* **2010**, *81*, 174103.

[5] a) M. C. Johnson, J. Wang, Z. Li, C. M. Lew, Y. Yan, *Mater. Sci. Eng. A* **2007**, *456*, 58; b) L. Brabec, P. Bohac, M. Stranyanek, R. Ctvrtlik, M. Kocirik, *Microporous Mesoporous Mater.* **2006**, *94*, 226; c) Z. A. D. Lethbridge, R. I. Walton, A. Bosak, M. Krisch, *Chem. Phys. Lett.* **2009**, *471*, 286.

[6] C. Lee, X. Wei, J. W. Kysar, J. Hone, *Science* **2008**, *321*, 385.

[7] a) D.-D. Zu, L. Lu, X.-Q. Liu, D.-Y. Zhang, L.-B. Sun, *J. Phys. Chem. C* **2014**, *118*, 19910; b) R. Kumar, K. Jayaramulu, T. K. Maji, C. N. R. Rao, *Chem. Commun.* **2013**, *49*, 4947; c) A. Huang, Q. Liu, N. Wang, Y. Zhu, J. Caro, *J. Am. Chem. Soc.* **2014**, *136*, 14686; d) Y. Hu, J. Wei, Y. Liang, H. Zhang, X. Zhang, W. Shen, H. Wang, *Angew. Chem. Int. Ed.* **2016**, *55*, 2048; *Angew. Chem.* **2016**, *128*, 2088.

[8] a) S. R. Caskey, A. G. Wong-Foy, A. J. Matzger, *J. Am. Chem. Soc.* **2008**, *130*, 10870; b) P. D. C. Dietzel, V. Besikiotis, R. Blom, *J. Mater. Chem.* **2009**, *19*, 7362.

[9] a) A. C. Kizzie, A. G. Wong-Foy, A. J. Matzger, *Langmuir* **2011**, *27*, 6368; b) J. Liu, A. I. Benin, A. M. B. Furtado, P. Jakubczak, R. R. Willis, M. D. LeVan, *Langmuir* **2011**, *27*, 11451.

[10] a) P. D. C. Dietzel, Y. Morita, R. Blom, H. Fjellvåg, *Angew. Chem. Int. Ed.* **2005**, *44*, 6354; *Angew. Chem.* **2005**, *117*, 6512; b) P. D. C. Dietzel, B. Panella, M. Hirscher, R. Blom, H. Fjellvag, *Chem. Commun.* **2006**, 959.

[11] N. L. Rosi, J. Kim, M. Eddaoudi, B. Chen, M. O'Keeffe, O. M. Yaghi, *J. Am. Chem. Soc.* **2005**, *127*, 1504.

[12] a) D. W. Mayo, F. A. Miller, R. W. Hannah in *Course notes on the interpretation of infrared and Raman spectra*, Wiley, New York, **2004**; b) K. Nakamoto, *Infrared and Raman spectra of inorganic and coordination compounds*, Wiley, Hoboken, **2009**.

[13] a) L. M. Malard, M. A. Pimenta, G. Dresselhaus, M. S. Dresselhaus, *Phys. Rep.* **2009**, *473*, 51; b) M. A. Pimenta, G. Dresselhaus, M. S. Dresselhaus, L. G. Cancado, A. Jorio, R. Saito, *Phys. Chem. Chem. Phys.* **2007**, *9*, 1276.

[14] a) T. Tsuruoka, S. Furukawa, Y. Takashima, K. Yoshida, S. Isoda, S. Kitagawa, *Angew. Chem. Int. Ed.* **2009**, *48*, 4739; *Angew. Chem.* **2009**, *121*, 4833; b) D. Li, H. Wang, X. Zhang, H. Sun, X. Dai, Y. Yang, L. Ran, X. Li, X. Ma, D. Gao, *Cryst. Growth Des.* **2014**, *14*, 5856; c) F. Wang, H. Guo, Y. Chai, Y. Li, C. Liu, *Microporous Mesoporous Mater.* **2013**, *173*, 181.

[15] a) W. Lu, W. M. Verdegaal, J. Yu, P. B. Balbuena, H.-K. Jeong, H.-C. Zhou, *Energy Environ. Sci.* **2013**, *6*, 3559; b) J. Zhang, Z.-A. Qiao, S. M. Mahurin, X. Jiang, S.-H. Chai, H. Lu, K. Nelson, S. Dai, *Angew. Chem. Int. Ed.* **2015**, *54*, 4582; *Angew. Chem.* **2015**, *127*, 4665; c) A. L. Myers, *Fundamental of Adsorption*, Engineering Foundation, New York **1986**.

[16] a) K. E. Prasad, B. Das, U. Maitra, U. Ramamurty, C. N. R. Rao, *Proc. Natl. Acad. Sci. USA* **2009**, *106*, 13186; b) Y. Chen, X. Zhang, E. Liu, C. He, C. Shi, J. Li, P. Nash, N. Zhao, *Sci. Rep.* **2016**, *6*, 19363; c) J. Liu, Y. Yang, H. Hassanin, N. Jumbu, S. Deng, Q. Zuo, K. Jiang, *ACS Appl. Mater. Interfaces* **2016**, *8*, 2607; d) J. Liu, H. Yan, K. Jiang, *Ceram. Int.* **2013**, *39*, 6215.

Received: April 9, 2016
Published online: June 10, 2016

